영상의학과 박사 학위논문

Quantitative Magnetic Resonance Imaging of Renal Parenchymal Disease: An Experimental In Vivo Study Using Rat Chronic Kidney Disease Models

신 실질 질환에서 정량적 자기공명영상의 유용성: 쥐 만성 신 질환 모델을 이용한 실험연구

2021 년 2 월

서울대학교 의과대학원
영상의학과 영상의학 전공
김 상 윤

영상의학과 박사 학위논문

Quantitative Magnetic Resonance Imaging of Renal Parenchymal Disease: An Experimental In Vivo Study Using Rat Chronic Kidney Disease Models

신 실질 질환에서 정량적 자기공명영상의 유용성: 쥐 만성 신 질환 모델을 이용한 실험연구

2020 년 10 월

서울대학교 의과대학원
영상의학과 영상의학 전공
김 상 윤

신 실질 질환에서 정량적 자기공명영상의 유용성: 쥐 만성 신 질환 모델을 이용한 실험연구

지도교수 조 정 연

이 논문을 영상의학과 박사 학위논문으로 제출함

2021 년 1 월

서울대학교 의과대학원

영상의학과 영상의학 전공

김 상 윤

김상윤의 박사 학위논문을 인준함

2021 년 1 월

위 원 장 주 권 욱 (인)

부 위 원 장 조 정 연 (인)

위 원 문 민 환 (인)

위 원 김 현 진 (인)

위 원 정 성 일 (인)

ABSTRACT

Quantitative Magnetic Resonance Imaging of Renal Parenchymal Disease: An Experimental In Vivo Study Using Rat Chronic Kidney Disease Models

Sang Youn Kim

Department of Radiology

Graduate School of Medicine

Seoul National University

Objective

This study aimed to validate the usefulness of quantitative multiparametric magnetic resonance imaging (MRI) sequence parameters and suggest the suitable spectroscopic metabolites in the evaluation of parenchymal fibrosis using an experimental animal model of chronic kidney disease (CKD) by long-term adenine intake.

Materials and Methods

Experimental adenine intake in rats induces renal dysfunction due to the deposition of 2,8-dihydroxyadenine crystals in the renal parenchyma. This pathophysiologic progression resembles that of human CKD. A total of 16 male Wistar rats were analyzed. They were divided into three groups: control (n = 7), CKD1 (n = 5), and CKD2 (n = 4). The CKD groups were kept under the 3- or 6-week term intake of 0.25% adenine. According to group assignment, quantitative MRI sequences, including diffusion-weighted image, T1ρ (T1 rho), T2* mapping, and in vivo MR spectroscopy (1H-MRS), were performed using a 9.4T animal MR scanner. A semiquantitative histopathologic analysis for renal fibrosis was conducted. Comparative analyses of quantitative MR values measured from anatomic regions of kidneys between groups were performed.

Results

Compared to the control group, significant histopathologic changes were observed in CKD groups according to periods. The apparent diffusion coefficient (ADC) and T1 (T1 rho) values were significantly increased in all CKD groups compared with those in the control group. The differences in values measured from the cortex and outer medulla were significant between all CKD groups and control group. The total ADC values tended to increase according to periods. The T1ρ (T1 rho) values were increased in the CKD1 group and decreased in the CKD2 group. Among MRS metabolites acquired from each region, the ratio of glycerophosphorylcholine–choline–phosphatidylcholine signals to myo-inositol–glycine signals collected from voxels located at medulla region was significantly lower in the CKD groups than in the control group (0.17 vs. 0.456, P = 0.0448).

Conclusion

Quantitative MRI sequences could be a noninvasive assessment modality in the diagnosis and evaluation of CKD. In particular, T1ρ may be a suitable MR sequence parameter to assess renal parenchymal fibrosis in a quantitative manner. Moreover, monitoring the change in common metabolites using MRS may reflect the alteration of osmolality in the renal medulla in CKD.

Keywords

Chronic kidney disease, Renal fibrosis, Magnetic resonance image, Diffusion magnetic resonance imaging, T2* magnetic resonance imaging, T1 rho magnetic resonance imaging, in vivo Magnetic resonance spectroscopy

Student Number: 2011-30538

Contents

List of Tables and Figures

collagen and other matrices (open arrowheads). Grade scales on interstitial fibrosis were also worse in the CKD2 group than in the CKD1 group (average grade scales of 2 and 4.2, respectively).

Figure 3. Representative histopathologic images (magnification, 200×) of kidneys stained with hematoxylin and eosin (H&E) and Masson's trichrome (MT). A semiquantitative grading method was applied for histopathologic evaluation. The degree of histopathologic changes was graded as six scales. The rats in control groups showed normal histologic findings (Grade 0). Instead, CKD rats by adenine intake showed significant increases in grades of renal fibrosis. H&E-stained images revealed tubular wall thinning and atrophy with tubular luminal dilatation. The accumulation of inflammatory cells was combined. The Bowman's space showed dilated, and the capillary lumen within glomerulus was obliterated. MT-stained images revealed that the interstitial space expanded and was occupied by collagen and other matrices (open arrowheads). Grade scales on interstitial fibrosis were worse in the CKD2 group than in the CKD1 group (average grade scales of 2 and 4.2, respectively).

Figure 4. Representative ADC images between three groups. The ADC values were significantly increased in all CKD groups induced by long-term adenine intake compared with those in the control group. The differences in values measured at the CO and OM were significantly apparent between all CKD groups and control groups. The total ADC values tended to increase according to periods. The differences were significant between the CKD1 and control groups. The differences were not significant between the CKD2 and CKD1 groups. The ADC values measured at the CO and OM showed a significant increase in the CKD1 group. The ADC values measured at the CO and OM of the CKD2 group were lower than those of the CKD1 group, but there was no statistical significance.

Figure 5. Representative T1 rho images between three groups. The total T1ρ values were significantly

increased in all CKD groups compared with those in the control group. The differences in values measured at the CO and OM were significantly apparent between all CKD groups and control groups. The T1ρ values were increased in the CKD1 group and decreased in the CKD2 group. The differences were significant between the CKD1 and control groups. The T1ρ values measured at the CO and OM of the long-term adenine intake group (CKD2) were lower than those of the short-term adenine intake group (CKD1).

Figure 6. Representative T2*mapping among the three groups. The total T2* values tended to show an increase in all CKD groups compared with those in the control groups. However, the differences were not statistically significant.

Figure 7. The ratio of Cho-containing compounds (glycerophosphorylcholine (GPC)–choline (Cho)–phosphatidylcholine (PC)) signals to myo-inositol (Ins)–glycine (Gly) signals measured in voxels delineated at medullae was lower in the CKD group. The ratio of Sor to Cho-containing compounds measured in voxels delineated at the medullae was higher in the CKD group.

Introduction

Chronic kidney disease (CKD) is a global health issue, and the prevalence rate of CKD has rapidly increased. A study published in 2016 revealed that the global prevalence of CKD was increased by 87% and the death rate from CKD was increased by 98% since 1990 [1]. In the USA, the estimated prevalence of CKD for adults was 15%. Older individuals aged ≥65 years showed higher prevalence (38%) than individuals aged 45–64 years (13%) or 18–44 years (7%) [2]. In Korea, the estimated prevalence of CKD for adults aged ≥20 years was 8.2% [3].

CKD is associated with high morbidity, premature mortality, and high-cost expenditure of healthcare [4]. Because the progression of CKD results in end-stage renal disease (ESRD) requiring dialysis or kidney transplantation, early detection, and assessment of stage are required to prevent disease progression. The progression of CKD is microscopically associated with the replacement of normal parenchyma into nonfunctioning tissues, such as glomerulosclerosis, tubular atrophy, and tubulointerstitial fibrosis [5]. Considering that parenchymal fibrosis is one of the major factors resulting in the progression of CKD and an important determinant of long-term disease outcome, assessment of fibrosis can help in the early detection and management of CKD [6, 7].

Although most evaluation methods of parenchymal fibrosis have been performed using direct tissue acquisition by percutaneous renal biopsy, renal biopsy is an invasive tool, and there is a risk of complications, such as massive bleeding, hematuria, and intrarenal vascular damage [8, 9]. Recent advances in magnetic resonance imaging (MRI) may allow it to be an alternative emerging tool for noninvasive evaluation of parenchymal fibrosis. Promising quantitative multiparametric MRI sequences, such as diffusion-weighted images (DWI), T1ρ (T1 rho), T2* mapping, and in vivo MR spectroscopy (1H-MRS), enable the evaluation of parenchymal fibrosis in vivo [10–16].

Currently, serial studies on the combination of renal fibrosis and MRI have been published. However, the optimal quantitative MR sequence parameters or spectroscopic metabolites used to assess renal fibrosis in the clinical field remain unclear. Thus, the goal of the present study was to validate the usefulness of quantitative multiparametric MRI sequence parameters and suggest the suitable spectroscopic metabolites in the evaluation of parenchymal fibrosis using an experimental animal model of CKD by long-term adenine intake.

Materials and Methods

Experimental Animal Model of CKD

Experimental adenine intake in rats induces the deposition of 2,8-dihydroxyadenine crystals in the renal parenchyma. It results in glomerulosclerosis, tubular atrophy, tubulointerstitial inflammation and fibrosis, and progressive kidney damage. This pathophysiologic progression resembles that of human CKD [17–19]. The experimental animal model was approved by the Animal Care and Use Committee of our institution (13-0377-C1A0). A total of 16 male Wistar rats aged 9–10 weeks weighing approximately 320 g were recruited and adapted for seven days before initiation of the experiment. Rats were kept under constant environment with free access to food and water. They were divided into three groups: control (n = 7), CKD1 (n = 5), and CKD2 (n = 4).

The image protocol consisted of a baseline MRI scan before adenine intake and an additional MRI scan according to group assignment (Fig. 1). The CKD1 group (n = 5) was kept under the 3-week term intake of 0.25% adenine by daily feeding 2 mL/kg adenine mixed fluid (100 mg/mL of adenine concentrations was adjusted with distilled water) using Zonde. The CKD2 group (n = 4) was kept under the 6-week term intake of 0.25% adenine [17–19]. At the end of the study period according to group assignment, all rats were anesthetized with ketamine/xylazine and sacrificed by exsanguination after blood sample was obtained from the abdominal aorta. Bilateral kidneys were harvested and fixed with formalin [18].

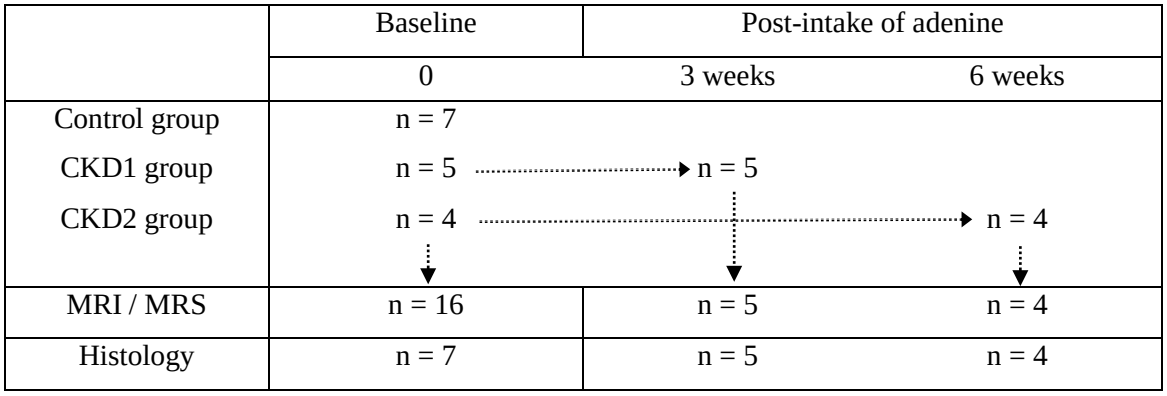

Figure 1. Diagram shows image protocol and assignment of rats to the three groups. The image protocol consisted of a baseline MRI scan before adenine intake and an additional MRI scan according to group assignment. Group 1 underwent short-term adenine intake for 3 weeks, and group 2 underwent long-term adenine intake for 6 weeks.

Histopathologic Analysis

The 32 kidney specimens were sliced in the coronal plane at the center and stained with hematoxylin and eosin (H&E) and Masson's trichrome (MT). H&E staining and MT staining were performed to evaluate parenchymal fibrosis. Analyses of kidneys were performed in a blinded fashion by an experienced veterinary pathologist (J.H.P.). The glomerulosclerosis presented by the dilatation of Bowman's space and thickening of the glomerular basement membrane, tubular atrophy, crystal deposition within the tubular lumen and giant cell, interstitial infiltration of inflammatory cells (lymphocyte, neutrophil, monocyte, and macrophage), and interstitial fibrosis were evaluated under magnification of 20× and 200× microscopic scales. A semiquantitative grading method was applied for histopathologic evaluation. The degree of histopathologic changes was graded as six scales based on the method suggested by Shackelford et al. [18, 20]. The details were as follows: Grade 0, no changes; Grade 1, up to 10% of the tissue in section is changed; Grade 2, between 11% and 20% of

the tissue in section is changed; Grade 3, between 21% and 40% of the tissue in section is changed; Grade 4, between 41% and 60% of the tissue in section is changed; and Grade 5, between 61% and 100% of the tissue in section is changed.

MR Data Acquisition

All MRI scans were conducted on a 9.4-T animal MR scanner (Agilent 9.4T/160AS imaging system, Agilent Technologies, CA, USA) with a volume coil (Agilent Technologies, CA, USA) for both radiofrequency transmission and signal reception. Before MR scan, rats were placed in a small chamber, anesthetized (1.5% isofluorane in 100% oxygen), and moved onto the animal bed inside the magnet. During MR scan, rats were continuously anesthetized (1% isofluorane in 100% oxygen), and their respiration and rectal temperature were monitored. The image protocol consisted of a baseline MRI scan before adenine intake and an additional MRI scan according to group assignment.

MRI

For DWI experiments, a respiratory-gated fast spin echo (FSE)-based DWI sequence was used. The diffusion gradient was applied along the readout direction with b values of 0/100/300/600/1000 s/mm2. The rest of the sequence parameters were as follows: repetition time (TR)/echo time (TE) = 3000/36 ms, flip angle (FA) = 90°/180°, 1 average, echo train length (ETL) = 8, echo spacing (ESP) = 9.2 ms, number of slices = 1 (coronal), slice thickness (TH) = 1.5 mm, field of view (FOV) = 50 × 50 mm2, matrix size = 128 × 128, and receiver bandwidth = 50 kHz.

For T1ρ (T1 rho) experiments, the rotary-echo spin locking preparation module was used in combination with a respiratory-gated FSE sequence [21]. The spin locking times (TSL) were 10/20/30/50/80 ms, and ω1 (=γB1) was 500 Hz. The rest of the sequence parameters were as follows: TR/TE = 2000/8.5 ms, FA = 90°/180°, 1 average, ETL = 4, number of slices = 1 (coronal), TH = 1.5 mm, FOV = 70 × 50 mm2, matrix size = 192 × 128, and receiver bandwidth = 50 kHz.

For T2* experiments, a respiratory-gated spoiled gradient echo sequence was used. The echo times were 2/5/10/15/20/25/30/35 ms. The rest of the sequence parameters were as follows: TR = 2000 ms, FA = 90°, 1 average, number of slices = 1 (coronal), TH = 1.5 mm, FOV = 70 × 50 mm2, matrix size = 192 × 128, and receiver bandwidth = 50 kHz.

In vivo-^{1}H-MRS

For the localization of MRS voxels, scout images were acquired in all three orthogonal directions using a respiratory-gated gradient echo sequence with the following sequence parameters: TR/TE = 79/2.7 ms; FA = 30°; 1 average; number of slices = 20 (axial), 7 (coronal), and 15 (sagittal); TH = 2 mm; FOV = 65 × 65 mm2; matrix size = 128 × 128; and receiver bandwidth = 50 kHz.

Kidney MRS spectra were collected from two voxels (outer medulla (OM) + inner medulla (IM) and cortex (CO) + OM) for each animal using a respiratory-gated spin echo full-intensity acquired localized spectroscopy (SPECIAL) sequence with the following sequence parameters: voxel size = 3 × 3 × 3 mm3, TE = 3.4 ms, (nominal) TR = 2000 ms, spectral width = 5000 Hz, number of data points = 2048, 256 average, and 32-step phase cycling. Water signal was suppressed by a VAPOR module [22, 23].

Quantitative MR imaging analysis

MRI

Apparent diffusion coefficient (ADC), T1ρ (T1 rho), and T2* maps were all calculated using MATLAB (MathWorks, Inc., Natick, MA, USA) by assuming a single exponential decay, i.e., exp(−TSL/T1ρ), exp(−b × ADC), and exp(−TE/T2*), respectively. After ADC, T1ρ (T1 rho), and T2* mapping images were generated, the values of the ADC, T1ρ (T1 rho), and T2* signals were

measured from CO, OM, and IM for each kidney. The regions of interest (ROIs) for measurement were placed on entire regions by free-hand drawing. All image analyses were performed by an experienced radiologist (S.Y.K., with 10 years of experience in MRI interpretation) blinded to information on group assignment.

In vivo-^{1}H-MRS

MRS data were analyzed using the linear combination model method (LCModel) (version 6.3-1J) [24]. The spectral basis set included the following metabolites: acetate (Act), alanine (Ala), aspartate (Asp), betaine (Bet), choline (Cho), glucose (Glc), glutamate (Glu), glutamine (Gln), glycerophosphorylcholine (GPC), glycine (Gly), isoleucine (ILc), lactate (Lac), leucine (Leu), lipid (Lip), lysine (Lys), myo-inositol (Ins), phenylalanine (PAl), phosphatidylcholine (PC), proline (Pro), sorbitol (Sor), taurine (Tau), threonine (Thr), trimethylamine N-oxide (TMAO), tyrosine (Tyr), and valine (Val). The basis spectra for Bet, ILc, Leu, Lys, PC, Pro, Sor, TMAO, and Tyr were simulated using General Approach to Magnetic Resonance Mathematical Analysis (GAMMA) by referring to the previously reported chemical shifts and J-coupling constants of the metabolites (http://www.hmdb.ca) [25, 26]. Only those data with Cramer–Rao lower bounds (CRLB) < 30% were included in the final data analysis.

Statistical analysis

The linear mixed model (LMM) was used to compare the quantitative MRI values between the three groups and the differences in measured values per region between groups. The Wilcoxon rank sum test was used to compare the MR spectroscopic metabolites between the control and CKD groups and the differences in measured values per region between the control and CKD groups.

P-value < 0.05 was considered statistically significant. Statistical analyses were performed using SAS software version 9.3 (SAS Institute, North Carolina, USA) and Stata software version 11.0 (Stata Corp., College Station, TX, USA).

Results

Histopathologic changes between control and CKD groups

Experimental adenine intake in rats induces the deposition of 2,8-dihydroxyadenine crystals in the renal parenchyma. It results in glomerulosclerosis, tubular atrophy, tubulointerstitial inflammation and fibrosis, and progressive kidney damage. This pathophysiologic progression resembles that of human CKD [17–19]. In our study, the histopathologic changes in the control group without adenine intake were unremarkable, and all grades were 0.

Compared to the control group, significant histopathologic changes were observed in CKD groups with adenine intake for 3 and 6 weeks. In CKD groups, deposition of dihydroxyadenine crystals in the renal tubules and interstitium was observed, and the grade scale was worse in CKD2 than in CKD1 (average grade scales of 5 and 2.5, respectively). Masson's trichrome-stained images revealed that the interstitial space widened and was occupied by collagen and other matrices. Grade scales of interstitial fibrosis were also worse in CKD2 than in CKD1 (average grade scales of 2 and 4.2, respectively). There was a significant progression of other histopathologic conditions, such as tubular dilatation, tubular atrophy, and interstitial nephritis, between the CKD1 and CKD2 groups (Table 1) (Figs. 2 and 3).

Table 1. Comparison of histopathologic changes among the three groups

Histopathologic Findings / Groups	Control	CKD1 (3Wk)	CKD2 (6Wk)
Deposition of dihydroxyadenine crystalline	0	2.5 (0.54)	5 (0)
Interstitial fibrosis	0	2 (0)	4.2 (0.45)
Tubular atrophy	0	2.25 (0.46)	4 (0)
Tubular dilatation	0	2.25 (0.46)	3 (0)
Interstitial nephritis	0	2.25 (0.46)	4.2 (0.45)
Crystal laden Giant cell	0	1 (0)	2.6 (0.55)
Dilated Bowman's space	0	1 (0)	2 (0)
Thickening of the glomerular basement membrane	0	0	2.2 (0.45)
Thickening of the tubular basement membrane	0	0	2.6 (0.55)

Note. A semi-quantitative grading method was applied for histopathologic evaluation. The degree of histopathologic changes was graded as 6 scales. All measurements are mean values (Standard deviations).

The CKD1 group was kept under the 3week term intake of 0.25% adenine. The CKD2 group was kept under the 6week term intake of 0.25% adenine.

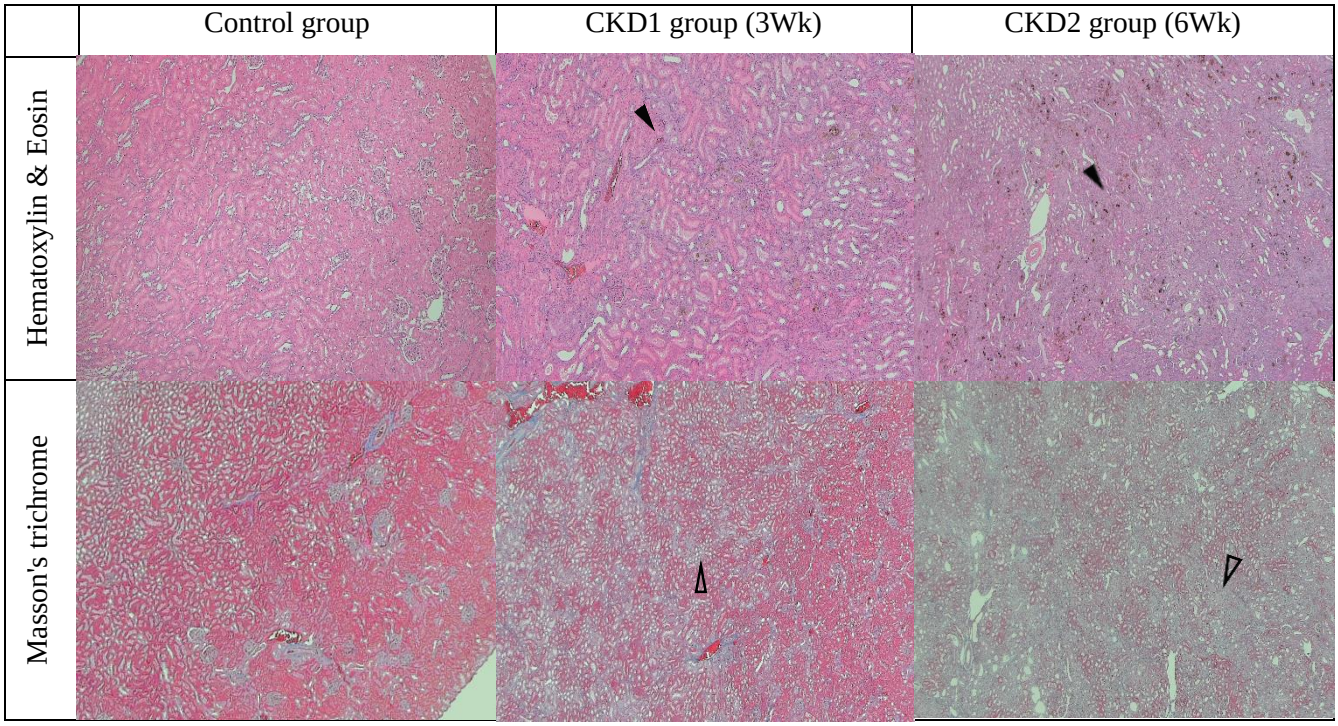

Figure 2. Representative histopathologic images (magnification, 20×) of kidneys stained with hematoxylin and eosin (H&E) and Masson's trichrome (MT). A semiquantitative grading method was applied for histopathologic evaluation. The degree of histopathologic changes was graded as six scales. The rats in control groups showed normal histologic findings (Grade 0). Instead, CKD rats by adenine intake showed significant increases in grades of renal fibrosis. H&E-stained images revealed deposition of dihydroxyadenine crystals in renal tubules and interstitium (arrowheads), and the grade scale was worse in the CKD2 group than in the CKD1 group (average grade scales of 5 and 2.5, respectively). MT-stained images revealed that the interstitial space expanded and was occupied by collagen and other matrices (open arrowheads). Grade scales on interstitial fibrosis were also worse in the CKD2 group than in the CKD1 group (average grade scales of 2 and 4.2, respectively).

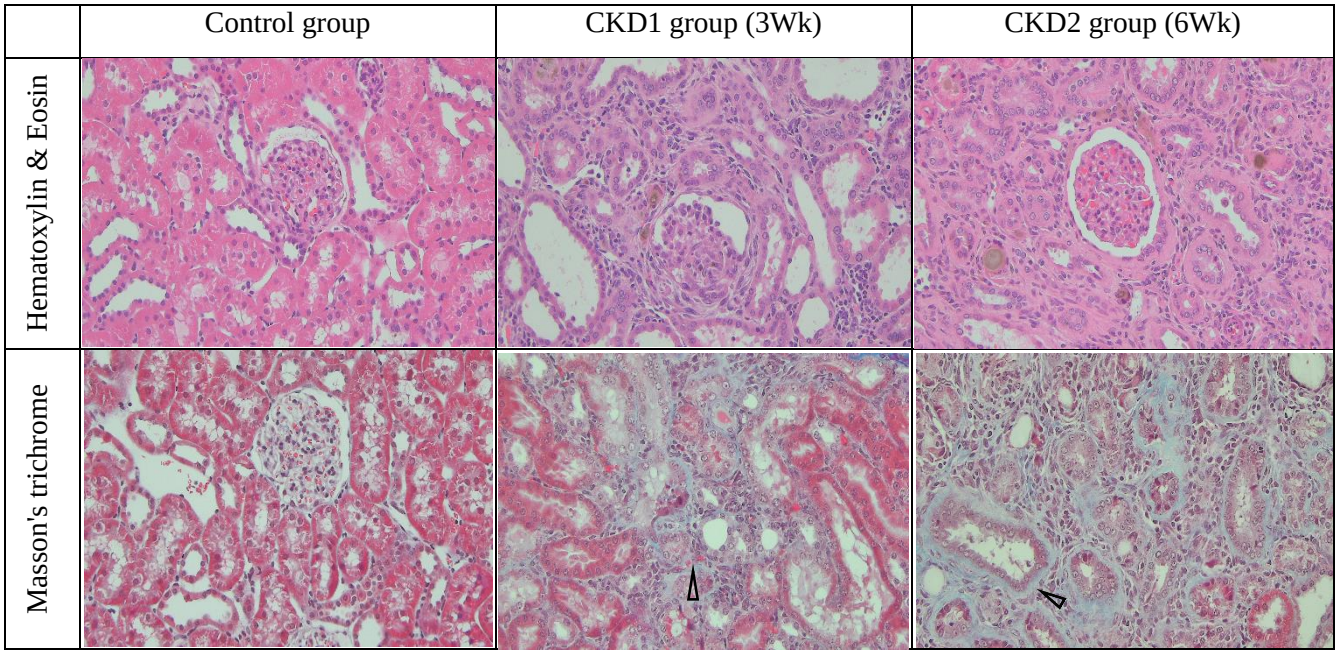

Figure 3. Representative histopathologic images (magnification, 200×) of kidneys stained with hematoxylin and eosin (H&E) and Masson's trichrome (MT). A semiquantitative grading method was applied for histopathologic evaluation. The degree of histopathologic changes was graded as six

scales. The rats in control groups showed normal histologic findings (Grade 0). Instead, CKD rats by adenine intake showed significant increases in grades of renal fibrosis. H&E-stained images revealed tubular wall thinning and atrophy with tubular luminal dilatation. The accumulation of inflammatory cells was combined. The Bowman's space showed dilated, and the capillary lumen within glomerulus was obliterated. MT-stained images revealed that the interstitial space expanded and was occupied by collagen and other matrices (open arrowheads). Grade scales on interstitial fibrosis were worse in the CKD2 group than in the CKD1 group (average grade scales of 2 and 4.2, respectively).

Comparison of quantitative MR sequence parameters between control and CKD groups

The comparisons of ADC, T1ρ, and T2* mapping parameters between the control and CKD groups are presented in Tables 2 and 3.

The ADC values were significantly increased in all CKD groups induced by long-term adenine intake compared with those in the control group. The differences in values measured at the CO and OM were significantly apparent between all CKD and control groups. The total ADC values tended to increase according to periods. The differences were significant between the CKD1 and control groups. The differences were not significant between the CKD2 and CKD1 groups. The ADC values measured at the CO and OM showed a significant increase in CKD1. The ADC values measured at the CO and OM of the CKD2 group were lower than those of CKD1, but there was no statistical significance (Fig. 4).

The total T1ρ values were significantly increased in all CKD groups compared with those in the control group. The differences in values measured at the CO and OM were significantly apparent between all CKD and control groups. The T1ρ values were increased in the CKD1 group and decreased in the CKD2 group. The differences were significant between the CKD1 and control

groups. The T1ρ values measured at the CO and OM in the CKD2 group were lower than those in the CKD1 group. The differences were significant (Fig. 5).

The total T2* values tended to increase in all CKD groups compared with those in the control groups. However, the differences were not statistically significant (Fig. 6).

Table 2. Pairwise comparison of ADC, T1ρ (T1 rho), and T2* mapping parameters among the three groups

MR parameters	Groups	Measurements	P value*	
			CKD1 (3Wk)	CKD2 (6Wk)
ADC($\times 10^{-3}mm^2/s$)	Control	1.238 (0.112)	<0.001	<0.001
	CKD1 (3Wk)	1.516 (0.120)		0.6044
	CKD2 (6Wk)	1.564 (0.122)		
T1 rho (ms)	Control	83.60 (18.22)	<0.0001	0.0894
	CKD1 (3Wk)	111.46 (18.49)		0.0160
	CKD2 (6Wk)	93.38 (18.63)		
T2* (ms)	Control	21.21 (3.68)	0.7213	0.1062
	CKD1 (3Wk)	21.82 (3.79)		0.2505
	CKD2 (6Wk)	24.19 (3.84)		

Note. All measurements are mean values (Standard deviations).

* The linear mixed model (LMM) method was used to compare the quantitative MRI values between the three groups, and the differences in values per each region between groups. A $P < 0.05$ was considered to be statistically significant.

The CKD1 group was kept under the 3week term intake of 0.25% adenine. The CKD2 group was kept under the 6week term intake of 0.25% adenine.

Table 3. Pairwise comparison of ADC, T1ρ (T1 rho), and T2* mapping parameters per region among the three groups

Anatomic regions	MR parameters	Groups	Measurements	P value*	
				CKD1 (3Wk)	CKD2 (6Wk)
Cortex	ADC ($\times 10^{-3} mm^2/s$)	Control	1.172 (0.082)	0.026	0.0311
		CKD1 (3Wk)	1.446 (0.099)		0.5137
		CKD2 (6Wk)	1.368 (0.103)		
	T1 rho (ms)	Control	47.30 (4.01)	<0.0001	0.0015
		CKD1 (3Wk)	77.36 (5.07)		0.01392
		CKD2 (6Wk)	66.70 (5.42)		
	T2* (ms)	Control	17.38 (0.95)	0.8835	0.4537
		CKD1 (3Wk)	17.26 (1.07)		0.4655
		CKD2 (6Wk)	18.10 (1.12)		
Outer Medullae	ADC ($\times 10^{-3} mm^2/s$)	Control	1.156 (0.093)	0.0048	0.0076
		CKD1 (3Wk)	1.488 (0.116)		0.9393
		CKD2 (6Wk)	1.477 (0.122)		
	T1 rho (ms)	Control	67.68 (6.20)	<0.0001	0.0055
		CKD1 (3Wk)	103.78 (7.00)		0.0133
		CKD2 (6Wk)	84.62 (7.27)		
	T2* (ms)	Control	19.61 (1.11)	0.5811	0.3771
		CKD1 (3Wk)	20.62 (1.45)		0.7421
		CKD2 (6Wk)	21.33 (1.57)		
Inner Medullae	ADC ($\times 10^{-3} mm^2/s$)	Control	1.485 (0.089)	0.0892	0.0075
		CKD1 (3Wk)	1.699 (0.116)		0.3771
		CKD2 (6Wk)	1.837 (0.121)		
	T1 rho (ms)	Control	139.84 (15.11)	0.2802	0.6183
		CKD1 (3Wk)	153.25 (16.38)		0.2325
		CKD2 (6Wk)	133.44 (17.65)		
	T2* (ms)	Control	27.20 (2.80)	0.8540	0.1816
		CKD1 (3Wk)	28.08 (3.81)		0.2978
		CKD2 (6Wk)	34.04 (4.14)		

Note. All measurements are mean values (Standard deviations).

* The linear mixed model (LMM) method was used to compare the quantitative MRI values between the three groups, and the differences in values per each region between groups. A $P < 0.05$ was considered to be statistically significant.

The CKD1 group was kept under the 3week term intake of 0.25% adenine. The CKD2 group was kept under the 6week term intake of 0.25% adenine.

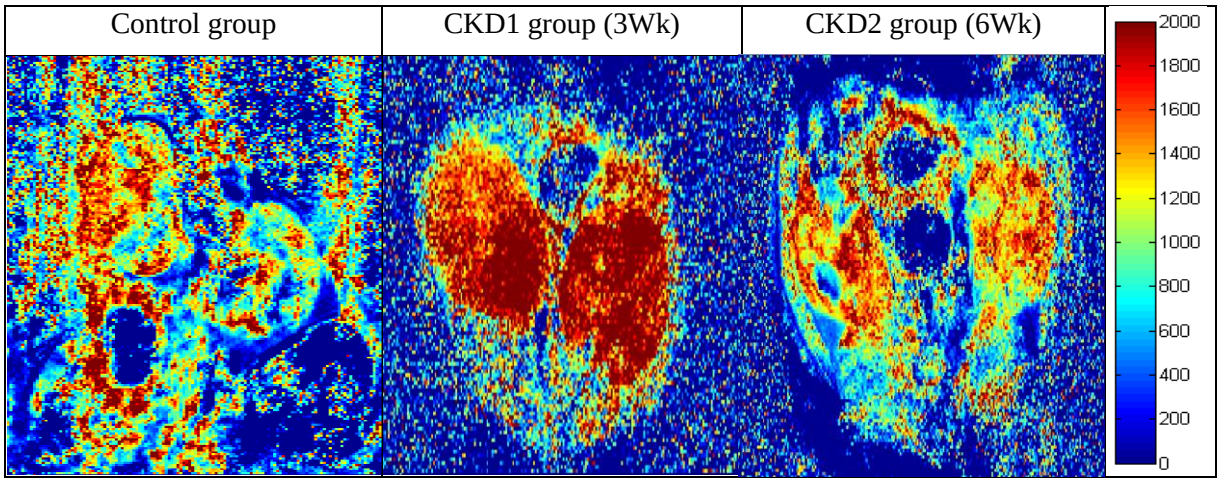

Figure 4. Representative ADC images between three groups. The ADC values were significantly increased in all CKD groups induced by long-term adenine intake compared with those in the control group. The differences in values measured at the CO and OM were significantly apparent between all CKD groups and control groups. The total ADC values tended to increase according to periods. The differences were significant between the CKD1 and control groups. The differences were not significant between the CKD2 and CKD1 groups. The ADC values measured at the CO and OM showed a significant increase in the CKD1 group. The ADC values measured at the CO and OM of the CKD2 group were lower than those of the CKD1 group, but there was no statistical significance.

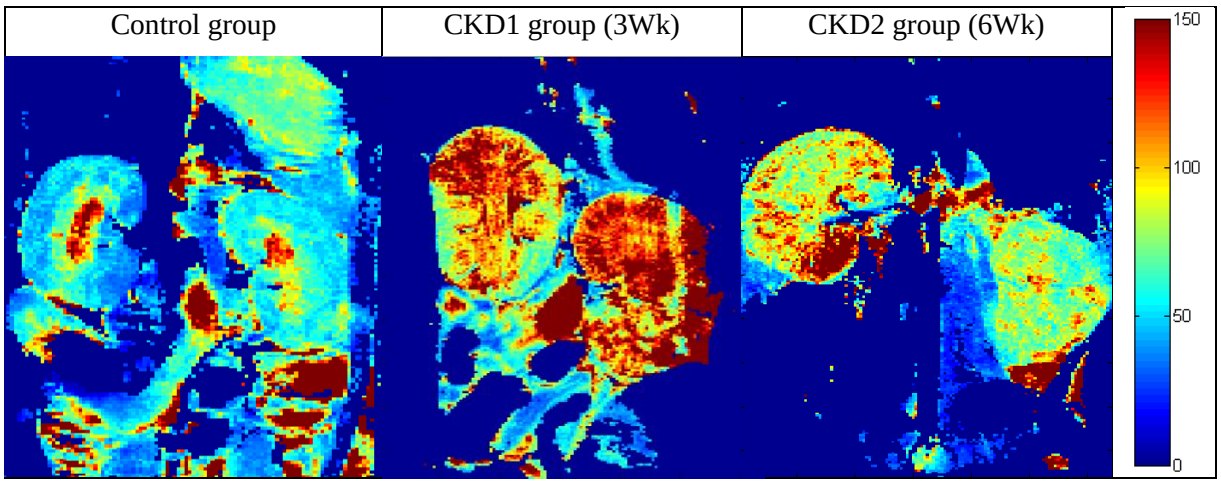

Figure 5. Representative T1 rho images between three groups. The total T1ρ values were significantly increased in all CKD groups compared with those in the control group. The differences in values measured at the CO and OM were significantly apparent between all CKD groups and control groups. The T1ρ values were increased in the CKD1 group and decreased in the CKD2 group. The differences were significant between the CKD1 and control groups. The T1ρ values measured at the CO and OM of the long-term adenine intake group (CKD2) were lower than those of the short-term adenine intake group (CKD1).

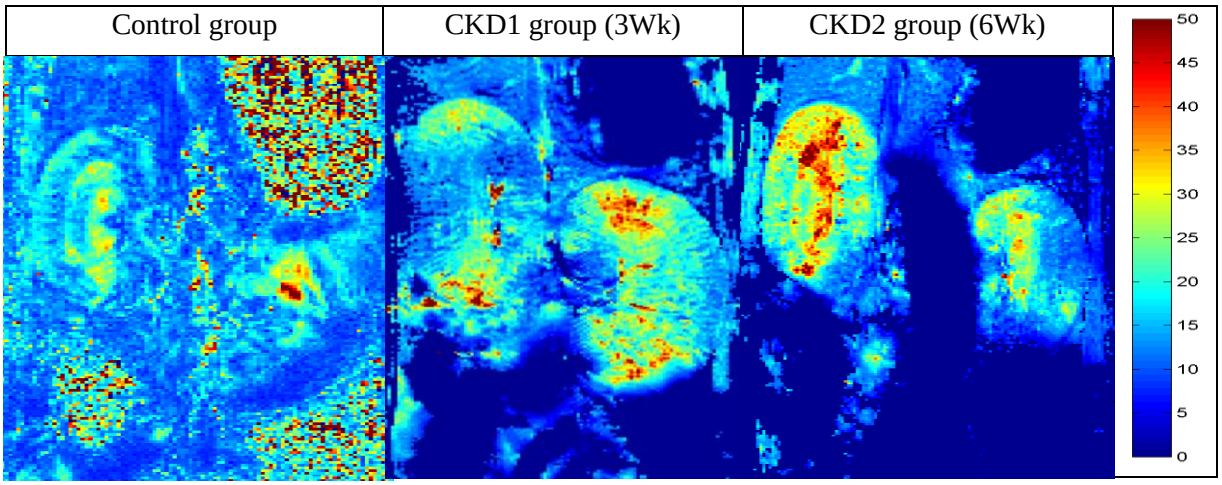

Figure 6. Representative T2*mapping among the three groups. The total T2* values tended to show an increase in all CKD groups compared with those in the control groups. However, the differences were not statistically significant.

Comparison of MRS metabolic values between control and CKD groups

The ratio of Cho-containing compounds (GPC–Cho–PC) signals to Ins–Gly signals measured in voxels delineated at the medulla (OM + IM) was significantly lower in all CKD groups than in the control group (0.17 vs. 0.456, P = 0.0448). The ratio of Sor signals to Cho-containing

compounds signals measured in voxels delineated at the medulla (OM + IM) was higher in all CKD groups than in the control group, but it was not statistically significant (1.32 vs. 0.331, P = 0.0805) (Fig. 7).

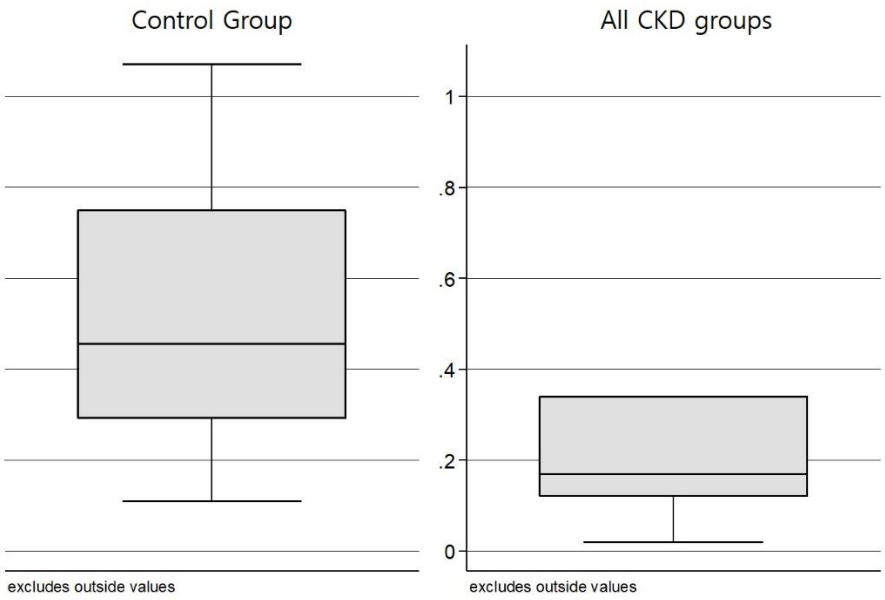

Figure 7. The ratio of Cho-containing compounds (glycerophosphorylcholine (GPC)–choline (Cho)–phosphatidylcholine (PC)) signals to myo-inositol (Ins)–glycine (Gly) signals measured in voxels delineated at medullae was lower in the CKD group. The ratio of Sor to Cho-containing compounds measured in voxels delineated at the medullae was higher in the CKD group.

Discussion

This study aimed to validate the usefulness of quantitative multiparametric MRI sequence parameters and MRS data during progression of renal parenchymal fibrosis in experimental rat CKD model by adenine intake. ADC values and T1ρ (T1 rho) values were significantly increased in all CKD groups compared with those in the control group. The differences in values measured from the CO and OM were significantly apparent between all CKD groups and control groups. The total ADC values tended to increase according to periods. The T1ρ (T1 rho) values were increased in CKD 1 and rather decreased in CKD2. Among MRS metabolites acquired from each region, the ratio of Cho-containing compounds to Ins, and Gly complex collected from voxels located at the medulla (OM + IM) was significantly lower in the CKD groups than in the control group. A major strength of this study is that we pursued the detailed image assessment of progression in renal fibrosis with quantitative multiparametric MRI sequence parameters.

The long intake of adenine in rats have been accepted as a model to research the causes and treatments of human CKD, because this manipulation resulted in most of the structural and functional changes seen in human CKD without the requirement for complex surgery. The long intake of adenine induced continuous progressive kidney damage with characteristic structural change of CKD. Pathophysiologically, involved kidneys showed tubular atrophy, erosion of proximal tubular brush borders with flattening of the tubular epithelium, interstitial inflammatory infiltrates, crystalline tubulointerstitial deposits, and glomerular injury, resembling a progression of human CKD [17-19].

Parenchymal fibrosis is an important contributor of CKD progression. Because the progression of fibrosis tends to have no manifestations, such as azotemia and elevation of blood pressure, until much of renal parenchyma have been replaced into nonfunctioning tissues, early detection, and interruption may prevent the development of renal dysfunction. Moreover, the

quantification of parenchymal fibrosis may help a nephrologist make a present decision and conduct future management of the remnant renal function [5–7, 27].

Although most evaluation methods of parenchymal fibrosis have been performed using direct tissue acquisition by percutaneous renal biopsy, renal biopsy is an invasive and limited tool. As mentioned earlier, renal biopsy has a risk of complications, such as massive bleeding, hematuria, and intrarenal vascular damage [8, 9]. As tissue acquisition is only 2 mm in diameter, <1% of one kidney, it cannot represent the entire situation of the relevant parenchyma. Moreover, needle biopsy almost never includes the medulla. Considering that the distribution of parenchymal fibrosis tends to be heterogeneous, the interpretation of the core biopsy on one side inherently increases the risks of sampling bias [27].

Recent advances in MRI may allow an alternative emerging solution for the evaluation of parenchymal fibrosis in a noninvasive manner. MRI analysis has the strength in that it evaluates both the renal CO and medulla. Numerous studies in both animal models and humans have shown remarkable performance for the evaluation of renal fibrosis in vivo [10–16]. In our study, we used promising quantitative multiparametric MRI sequence parameters, including ADC, T1ρ (T1 rho), T2* mapping, and 1H-MRS, to evaluate parenchymal fibrosis in vivo.

DWI is a MR technique that measures the Brownian motion of intra- and extracellular water molecules, via “diffusion weighting.” This weighting is reflected in the b value. The higher b values show more sensitivity to the motion of water molecules. The ordinarily used DWI metric is the ADC, which expresses both random diffusions and directed flows of water into a quantitative parameter [27]. Since Togao et al. [28], in which the authors mentioned that ADC values showed decrease according to the progression of parenchymal fibrosis after ligation of unilateral ureter in an animal model, it has been well accepted that ADC may serve as a useful biomarker of renal fibrosis. They reported that the decrease in ADC was due to the increase in cell density. Increased cell density results in the motion restriction of interstitial water molecules, and it leads to “diffusion restriction” [28, 29].

In a recent experimental study, ADC showed inverse correlation with the boundary of fibrosis and cell density [30]. As the accumulation of inflammatory cells, such as lymphocyte, neutrophils, monocyte, and macrophage, due to interstitial nephritis often appears in renal fibrosis and the increase in myofibroblast is associated with interstitial fibrosis, it can be asserted that the increase in cell density may be one of the main changes in the progression of renal fibrosis [5–7]. The decrease in ADC in CKD may be attributed to the increased cell density, cell swelling by impairment of cell membrane integrity, and/or decreased internal perfusion, leading to restriction of water molecules in the interstitial space. Another rationale for the decrease in ADC is that the accumulation of collagen and other matrix components may restrict the diffusion of water molecules [16, 31].

In human studies, the evaluation of ADC in vivo has been proven as a valuable imaging biomarker in detecting renal allograft dysfunction and renal deterioration in CKD and diabetic nephropathy, in which ADC values showed a positive correlation with renal function and an inverse correlation with tubulointerstitial injury [10, 32–35]. In our study, the total ADC values were significantly increased in all CKD groups induced by long-term intake of adenine compared with those in the control group. The differences in values measured at the CO and OM were significantly apparent between all CKD groups and control groups. The total ADC values tended to increase according to periods. The differences were significant between the CKD1 and control groups. The ADC values measured at the CO and OM of the 6-week adenine intake group (CKD2) were lower than those of the 3-week adenine intake group (CKD1), but it was not statistically significant. Our results were in line with those of Boor et al. and Schley et al. The renal CO is composed mostly of highly organized and differentiated columnar tubular cells, and the space occupied by the tubular lumen and interstitium is minimal. In fibrosis, tubular cells show flattening, and profound atrophy. As the space occupied by the cellular components is markedly diminished, it results in the dilation of the tubular lumen and expansion of the interstitial space. Although the overall cell count is increased by the inflammatory process and myofibroblastic proliferation, the overall occupied space by increased cells cannot replace the previous one occupied by tubular renal cells. According to Boor et al., the best

correlations were detected between postmortem ADC and measures of tubular dilation and interstitial expansion [36, 37]. It can also be assumed that the regression of acute tissue edema influenced an increase in ADC value in the late phase.

T1ρ, also known as T1 rho or "spin-lock" ("ρ" is the symbol for the Greek letter rho), is an MRI sequence that is proposed for the evaluation of cartilage in musculoskeletal imaging. T1ρ is dependent on T1 and T2 of the tissue, but changing the amplitude of the spin locking pulse can also allow the selection for different properties within the tissue (e.g., slow motion in the lattice such as proteins and collagen). T1ρ is sensitive for low-frequency interactions between macromolecules and bulk water [38].

Because T1ρ is sensitive to the presence of macromolecules, such as proteins and collagen, which show static processes and slow motions, T1ρ MRI enables monitoring and quantifying the accumulation of macromolecular contents, such as collagen, in parenchymal fibrosis. Its principle is that once the spin magnetization is tilted into the transverse plane and a pulse is applied, the magnetization gets into a spin-lock state and rotates at the frequency of the pulse. The following monoexponential decay of magnetization is recorded by imaging at different spin-lock times. The relaxation constant associated with this decay is named T1ρ [16, 39].

A recent study showed that T1ρ MR imaging can evaluate liver fibrosis, and the degree of fibrosis shows a positive correlation with the degree of the T1ρ measurements, suggesting that liver T1ρ quantification may take a leading role in the detection and grading of liver fibrosis. Another experimental study using rat model revealed that the degree of fibrosis is correlated with T1 rho values and that T1ρ MRI enables to monitor liver fibrosis degree [40, 41]. In another study using T1ρ in the evaluation of myocardial disease, T1ρ was sensitive to edema in an acute setting and a scar in chronic myocardial infarction. The abnormal zone in T1ρ mapping was correlated with that of a tissue section positively stained by MT. T1ρ was found to have improved contrast compared to T2 MRI between a scar and myocardial tissue because of the suppression of the low-frequency contributions to

the relaxation rate [42].

The applications of T1ρ MR imaging in renal parenchymal evaluation have not yet been widely reported. Because the accumulation of collagen and other matrix components also appears in renal fibrosis, T1ρ quantification may play the same role as those for the liver and heart [5–7]. In a recent experimental study using a rat CKD model by unilateral ureteral ligation, T1ρ values were correlated with the α-SMA protein levels and the percentages of areas positively stained with MT per tissue section. In another recent study for the evaluation of renal fibrosis in transplanted kidney, there was a significant difference in cortical T1ρ values between functional and fibrotic transplanted kidneys. They found that T1ρ values acquired from the CO in an allograft showed a positive correlation with collagen content measured histopathologically [43, 44]. Our results were in line with those of previous studies. In our study, the total T1ρ values were significantly increased in all CKD groups compared with those in the control group. The differences in values measured at the CO and OM were significantly apparent between all CKD groups and control groups. The T1ρ values were increased in the CKD1 group and decreased in the CKD2 group. The differences were significant between the CKD1 and control groups. The T1ρ values measured at the CO and OM of the long adenine intake group (CKD2) were lower than those of the short adenine intake group (CKD1). T1ρ values may represent the accumulation of collagen and other macromolecules in the progression of renal parenchymal fibrosis. T1ρ may be affected by tissue edema and cellular swelling. It can be assumed that the regression of acute tissue edema and cellular swelling influenced a decrease in the T1ρ value. In previous experimental animal studies on liver fibrosis monitored with T1ρ MRI, the T1ρ values acquired from rats with 4-week carbon tetrachloride intoxication were lower than those from rats with 2-week carbon tetrachloride intoxication, which was consistent with our results [45].

T2* mapping is an MRI sequence that is sensitive on magnetic field inhomogeneity. Magnetic field inhomogeneity may be caused by deoxyhemoglobin, blood products, or paramagnetic contrast agents in vessels. The magnetic properties of hemoglobin affect the T2* relaxation time of

the neighboring water molecules and lead to the MR signal changes on T2* mapping. Because tissue oxygenation is associated with the proportion of oxyhemoglobin to deoxyhemoglobin in the blood, the signal changes in the T2* mapping sequence can be interpreted as changes in tissue oxygenation. Because hypoxia is one of the main constituent in the pathophysiology of CKD, the quantification using T2* mapping can be a potential method for renal parenchymal evaluation [46, 47].

In our study, the total T2* values tended to increase in all CKD groups compared with those in control groups. However, the differences were not statistically significant. Our results were in line with those of previous studies. Inoue et al. reported that T2* relaxation time showed the inverse correlation with glomerular filtration rate in CKD patients. Woo et al. found that T2* relaxation time was significantly associated with the area of fibrosis. In a previous study using a diabetic mouse model, T2* mapping parameters (R2*) were sensitive in the evaluation of progressive changes of hypoxia [10, 30, 48].

MRS, also known as nuclear magnetic resonance spectroscopy, is a noninvasive, ionizing-radiation-free analytical technique. The technique of MRS has been used in chemistry for the analysis of compounds in solution. MRS enables the noninvasive measurement of relative concentrations of different biochemical components within tissues (metabolites), which are displayed as a spectrum with peaks consistent with various chemicals detected. Special MR Pulse sequences are applied to generate spectroscopic data within the appropriate anatomical location and volume (defined by voxels) of interest. The spectral analysis needs post-processing to reduce noise and perform analysis. Metabolite concentrations may be displayed in absolute or relative terms. In clinical use, the peak area of the metabolite signal reflects its concentration. ^{1}H (proton)-based MRS is widely used for the quantification because of the high natural abundance of protons and their high absolute sensitivity to magnetic manipulation, better spatial resolution, and relative simplicity of the technique [49, 50].

In vivo ^{1}H MRS has not been widely used for the evaluation of renal parenchymal fibrosis. The relative concentration of the metabolites in the human kidney is unclear. The application of in

vivo ^{1}H MRS in the kidney has technical limitations due to physiologic movement by respiration, peristalsis, or aortic pulsation. Renal motion may result in voxel misregistration, voxel contamination by perirenal fat, and poor reproducible data. In the initial application of in vivo ^{1}H MRS, we had some considerable technical difficulties for motion correction, shimming, frequency, and phase correction.

In our study, the remarkable metabolite complex was Ins–Gly, Cho-containing compounds (GPC–Cho–PC), and Sor. The relative concentration of these metabolite complexes showed high consistency in kidneys of all groups. Quantification of the metabolite could not be conducted because the peak signals of the metabolites overlap. In a previous study using bovine kidney, the relative concentration of these metabolites showed high consistency. Although the results of the MRS data from rat kidney may not be applied entirely to the assessment of human study, the similarities with extracts of rat and bovine kidneys suggest that these metabolites may be common in many mammal species. A previous study also reported that cells in the renal medullas of mammals contain large amounts of organic osmolytes, including Cho-containing compounds (GPC), Ins, Gly, Bet, and Tau [51–53].

Ins is associated with osmotic regulation in kidney. Ins functions as an organic osmolyte that enables renal cells to constantly adapt to hyperosmotic environments. In previous studies using diabetic animal models, depletion of Ins was proposed as one of the biologic markers of diabetic nephropathy. Renal depletion of Ins and accumulation of Sor may be associated with the Sor–Ins hypothesis, which has been proposed as one of the pathogenesis in diabetic nephropathy. In diabetes, depletion of Ins was proposed to arise as a consequence of the increased activity of the polyol pathway, whereby glucose is first converted to Sor by aldose reductase and then to fructose by Sor dehydrogenase. The elevated intracellular Sor levels caused a decrease in Ins level. Chang et al. reported that the depletion of Ins is correlated with the activity of myo-inositol oxygenase (MIOX), which is the Ins-catabolizing enzyme. Recent studies proposed that overactivation of MIOX in diabetic nephropathy can accelerate tubulointerstitial injury and fibrosis by oxidant and endoplasmic

reticulum stress [54–57].

Cho-containing compounds – Cho, GPC, and PC – are representative molecules in the synthesis and degradation of phospholipids, which are essential components of different membranes. In a previous MRS study on chronic liver disease, significant depletion of Cho-containing compounds was detected in cirrhotic liver tissue compared with noncirrhotic liver tissue. The literature proposed that considering the characterization of liver cirrhosis is the replacement of liver tissue by fibrous scar tissue, the depletion in Cho-containing compounds may reflect the decreased membrane turnover. In vivo ^{1}H-MRS has not been widely used for the evaluation of renal parenchymal fibrosis [58]. Some studies reported the usefulness of MRS for the differentiation of renal tumors.

In our study, the ratio of Cho-containing compounds to the Ins–Gly signal measured in voxels delineated at the medullae was lower in the CKD group. The ratio of Sor to choline-containing compounds measured in voxels delineated at the medullae was higher in the CKD group. Our results were in line with that of a previous study using renal aqueous extract analyses [59]. Zhong et al. found that the levels of GPC, Ins, Bet, and Tau acquired from an aqueous extract of rats with 5/6 nephrectomy significantly decreased whereas glycine level dramatically increased. Our results may reflect the change in renal medullary osmolality in case of CKD [59, 60].

In the present study, we could not apply magnetic resonance elastography (MRE) as a quantification tool because of technical limitation. The MRE technique is a costly noninvasive quantitative modality for the evaluation of parenchymal fibrosis in abdominal organs, such as the liver and kidney. MRE appears to be an alternative tool to ultrasound-based elastography. In this technique, an MRI pulse sequence is synchronized to tissue motion, and the propagation of mechanical shear waves can be detected in the tissue. The quantification of tissue stiffness can be evaluated by the detection of microscopic tissue displacement through the imaging volume. This technique was proposed to measure hepatic parenchymal fibrosis, but recent studies on its application in the kidney are presently reported. In a kidney MRE study using an animal CKD model, elastography results were

variable, and showed a weak correlation with the severity of fibrosis on histology. The studies proposed that several factors other than fibrosis might affect measured stiffness data. The published human renal studies on MRE have focused on proof of concept and reproducibility [31, 61–63].

One of the strengths of our study is that MRI scans and MRS data acquisition were performed in vivo before kidney harvest. In a recent similar study on MR evaluation of CKD, MRI scans were performed ex vivo to avoid motion and artifacts that may interfere with measurements [37]. However, it is difficult to conclude that ex vivo MR data obtained from formaldehyde-fixed specimens or aqueous extracts reflect in vivo data as it is. Formaldehyde fixation may alter water distribution in parenchymal tissue and affect diffusion property and metabolite ingredient. Shepherd et al. found that there were significant alterations in T1 and T2 times and ADC values after formaldehyde fixation of murine brain CO slices. Quantitative MR data acquired from formaldehyde-fixed kidney samples need to be interpreted with caution [64].

There are several limitations to this study. First, the sample size was small. Larger sample sizes may prevent statistical misinterpretation. A large sample size study in the future will be needed to evaluate a conclusive correlation between quantitative MR values and renal parenchymal fibrosis. Second, the acquisition and correlation of biochemical data including serum analysis was not performed in this study. In our study, we focused on the evaluation of quantitative MRI sequence parameters to reflect histopathological changes in CKD. Third, because of technical limitations, it was impossible to exactly match the regions of histopathologic and radiologic assessment. Moreover, the histopathologic analysis was a semiquantitative method. Fourth, MRI and MRS data were acquired in a single coronal slice to guarantee reproducible data acquisition and correct technical issues (i.e., rapid respiratory and cardiac rates, and motion and noise correction). It may preclude data acquisition from the total renal volume. Lastly, the ROIs for collecting MRS data were not delineated separately by region in the CO, OM, and IM. Because renal parenchymal layers were too thin for delineation of a 3 mm voxel, which needs to be conducted for stable MRS data acquisition, in a future study using an

advanced technique, it is expected that in vivo MRS analysis by kidney anatomical region can be performed.

In conclusion, quantitative MRI sequences provide potential as a noninvasive assessment modality for the diagnosis and evaluation of CKD. In particular, T1ρ may be a suitable MR sequence parameter in the assessment of renal parenchymal fibrosis in a quantitative manner. After validation in future studies, it can be a robust parameter that can be used on patients as well. Monitoring the change in common metabolites using MRS may reflect the alteration of osmolality in the renal medulla in CKD. Further validation in human clinical research is needed.

Acknowledgment

None of the authors have a conflict of interest or anything to disclose. This research was supported by a grant from the Seoul National University Hospital Research Fund (04-2011-0250)

References

1. Xie Y, Bowe B, Mokdad AH, et al. Analysis of the Global Burden of Disease study highlights the global, regional, and national trends of chronic kidney disease epidemiology from 1990 to 2016. Kidney Int 2018;94:567-581.

2. Centers for Disease Control and Prevention. Chronic Kidney Disease Surveillance System website. https://nccd.cdc.gov/CKD. Accessed January 7, 2019.

3. Park JI, Baek H, Jung HH. Prevalence of chronic kidney disease in Korea: The Korean National Health and Nutritional Examination Survey 2011–2013. J Korean Med Sci 2016;31:915-923.

4. Go AS, Chertow GM, Fan D, McCulloch CE, Hsu C. Chronic kidney disease and the risks of death, cardiovascular events, and hospitalization. N Engl J Med 2004;351:1296-1305.

5. Liu Y. Cellular and molecular mechanisms of renal fibrosis. Nat Rev Nephrol 2011;7:684-696.

6. Nath KA. Tubulointerstitial changes as a major determinant in the progression of renal damage. Am J Kidney Dis 1992;20:1-17.

7. Fogo AB. Mechanisms of progression of chronic kidney disease. Pediatr Nephrol 2007;22:2011-2022.

8. Bakdash K, Schramm KM, Annam A, et al. Complications of percutaneous renal biopsy. Semin Intervent Radiol 2019;36:97-103.

9. Trajceska L, Severova-Andreevska G, Dzekova-Vidimliski P, et al. Complications and risks of

percutaneous renal biopsy. Open Access Maced J Med Sci 2019;7:992-995.

10. Inoue T, Kozawa E, Okada H, et al. Noninvasive evaluation of kidney hypoxia and fibrosis using magnetic resonance imaging. J Am Soc Nephrol 2011;22:1429-1434.

11. Takahashi T, Wang F, Quarles CC. Current MRI techniques for the assessment of renal disease. Curr Opin Nephrol Hypertens 2015;24:217-223.

12. Mahmoud H, Buchanan C, Francis ST, Selby NM. Imaging the kidney using magnetic resonance techniques: structure to function. Curr Opin Nephrol Hypertens 2016; 25:487-493.

13. Berchtold L, Friedli I, Vallee JP, et al. Diagnosis and assessment of renal fibrosis: the state of the art. Swiss Med Weekly 2017;147:w14442.

14. Li J, An C, Kang L, Mitch WE, Wang Y. Recent Advances in Magnetic Resonance Imaging Assessment of Renal Fibrosis. Adv Chronic Kidney Dis 2017;24:150-153.

15. Delphine B, François S, Thierry H. Magnetic Resonance Spectroscopy (MRS) in kidney transplantation: Interest and perspectives. Magnetic Resonance Spectroscopy edited by DH Kim. 2012 published by InTech.

16. Petitclerc L, Gilbert G, Nguyen BN, Tang A. Liver Fibrosis Quantification by Magnetic Resonance Imaging. Top Magn Reson Imaging 2017;26:229-241.

17. Shuvy M, Nyska A, Beeri R, et al. Histopathology and apoptosis in an animal model of reversible renal injury. Exp Toxicol Pathol 2011;63:303-306.

18. Diwan V, Mistry A, Gobe G, Brown L. Adenine-induced chronic kidney and cardiovascular damage in rats. J Pharmacol Toxicol Methods 2013;68:197-207.

19. Diwan V, Brown L, Gobe GC. Adenine-induced chronic kidney disease in rats. Nephrology (Carlton) 2018;23:5-11.

20. Shackelford C, Long G, Wolf J, Okerberg C, Herbert R. Qualitative and quantitative analysis of nonneoplastic lesions in toxicology studies. Toxicol Pathol 2002;30:93-96.

21. Charagundla SR, Borthakur A, Leigh JS, Reddy R. Artifacts in T(1rho)-weighted imaging: correction with a self-compensating spin-locking pulse. J Magn Reson 2003;162:113-121.

22. Mlynárik V, Gambarota G, Frenkel H, Gruetter R. Localized short-echo-time proton MR spectroscopy with full signal-intensity acquisition. Magn Reson Med 2006;56:965-97023. Tkác I, Starcuk Z, Choi IY, Gruetter R. In vivo 1H NMR spectroscopy of rat brain at 1 ms echo time. Magn Reson Med 1999;41:649-656.

24. Provencher SW. Estimation of Metabolite Concentrations From Localized in Vivo Proton NMR Spectra. Magn Reson Med 1993;30:672-679.

25. Smith SA, Levante TO, Meier BH, Ernst RR. Computer-simulations in Magnetic-Resonance - An object-oriented programming approach. J Magn Reson Ser A 1994;106:75-105.

26. Garrod S, Humpfer E, Spraul M, et al. High-resolution magic angle spinning 1H NMR spectroscopic studies on intact rat renal cortex and medulla. Magn Reson Med 1999;41:1108-1118.

27. Leung G, Kirpalani A, Szeto SG, et al. Could MRI be used to image kidney fibrosis? A review of recent advances and remaining barriers. Clin J Am Soc Nephrol 2017;12:1019-1028.

28. Togao O, Doi S, Kuro-o M, et al. Assessment of renal fibrosis with diffusion-weighted MR imaging: study with murine model of unilateral ureteral obstruction. Radiology 2010;255:772-780.

29. Szafer A, Zhong J, Gore JC. Theoretical model for water diffusion in tissues. Magn Reson Med 1995;33:697-712.

30. Woo S, Cho JY, Kim SY, Kim SH. Intravoxel incoherent motion MRI-derived parameters and T2* relaxation time for noninvasive assessment of renal fibrosis: An experimental study in a rabbit model of unilateral ureter obstruction. Magn Reson Imaging 2018;51:104-112.

31. Morrell GR, Zhang JL, Lee VS. Magnetic resonance imaging of the fibrotic kidney. J Am Soc Nephrol 2017;28:2564-2570.

32. Thoeny HC, Zumstein D, Simon-Zoula S, et al. Functional evaluation of transplanted kidneys with diffusion-weighted and BOLD MR imaging: initial experience. Radiology. 2006;241:812-821.

33. Thoeny HC, De Keyzer F. Diffusion-weighted MR imaging of native and transplanted kidneys. Radiology 2011;259:25-38.

34. Cakmak P, Yağcı AB, Dursun B, Herek D, Fenkçi SM. Renal diffusion-weighted imaging in diabetic nephropathy: Correlation with clinical stages of disease. Diagn Interv Radiol 2014;20:374-378.

35. Hueper K, Khalifa AA, Bräsen JH, et al. Diffusion-Weighted imaging and diffusion tensor imaging detect delayed graft function and correlate with allograft fibrosis in patients early after kidney transplantation. J Magn Reson Imaging 2016;44:112-121.

36. Boor P, Perkuhn M, Weibrecht M, et al. Diffusion-weighted MRI does not reflect kidney fibrosis in a rat model of fibrosis. J Magn Reson Imaging 2015;42:990-998.

37. Schley G, Jordan J, Ellmann S, et al. Multiparametric magnetic resonance imaging of experimental chronic kidney disease: A quantitative correlation study with histology. PLoS One 2018;13:1-18.

38. Wang L, Regatte RR. Regatte Basic principles of T1 rho MRI and its application of musculoskeletal system. J Magn Reson Imaging 2015;41:586-600.

39. Gilani IA, Sepponen R. Quantitative rotating frame relaxometry methods in MRI. NMR Biomed 2016;29:841-861.

40. Zhao F, Yuan J, Deng M, Lu PX, Ahuja AT, Wang YX. Further exploration of MRI techniques for liver T1rho quantification. Quant Imaging Med Surg 2013;3:308-315.

41. Wang YX, Yuan J, Chu ES, et al. T1rho MR imaging is sensitive to evaluate liver fibrosis: an experimental study in a rat biliary duct ligation model. Radiology 2011;259:712-719.

42. Han Y, Liimatainen T, Gorman RC, Witschey WR. Assessing myocardial disease using T1rho MRI. Curr Cardiovasc Imaging Rep 2014;7:9248.

43. Hu G, Liang W, Wu M, et al. Comparison of T1 mapping and T1rho values with conventional diffusion-weighted imaging to assess fibrosis in a rat model of unilateral ureteral obstruction. Acad Radiol 2019;26:22-29.

44. Hectors SJ, Bane O, Kennedy P, et al. T1ρ mapping for assessment of renal allograft fibrosis. J Magn Reson Imaging 2019;50:1085-1091.

45. Xie S, Qi H, Li Q, et al. Liver injury monitoring, fibrosis staging and inflammation grading using T1rho magnetic resonance imaging: an experimental study in rats with carbon tetrachloride intoxication. BMC Gastroenterol. 2020;20:14.

46. Prasad PV, Edelman RR, Epstein FH. Noninvasive evaluation of intrarenal oxygenation with BOLD MRI. Circulation 1996;94:3271-3215.

47. Fine LG, Orphanides C, Norman JT. Progressive renal disease: The chronic hypoxia hypothesis. Kidney Int Suppl 1998;65:S74-S78.

48. Prasad P, Li LP, Halter S, et al. Evaluation of renal hypoxia in diabetic mice by BOLD MRI. Invest Radiol 2010;45:819-822.

49. Gujar SK, Maheshwari S, Bjorkman-Burtscher I, et al. Magnetic resonance spectroscopy. J Neuroophthalmol 2005;25:217-226.

50. Burtscher IM, Holtas S. Proton MR spectroscopy in clinical routine. J Magn Reson Imaging 2001;13:560-567.

51. Junankar PR, Kirk K. Organic osmolyte channels: a comparative view. Cell Physiol Biochem.

2000;10:355-360.

52. Bagnasco S, Balaban R, Fales HM, Yang YM, Burg M. Predominant osmotically active organic solutes in rat and rabbit renal medullas. J Biol Chem 1986;261:5872-5877.

53. Dixon RM, Frahm J. Localized proton MR spectroscopy of the human kidney in vivo by means of short echo time STEAM sequences. Magn Reson Med 1994;31:482-487.

54. Chang HH, Chao HN, Walker CS, Choong SY, Phillips A, Loomes KM. Renal depletion of myo-inositol is associated with its increased degradation in animal models of metabolic disease. Am J Physiol Renal Physiol 2015;309:F755-F763.

55. Croze ML, Soulage CO. Potential role and therapeutic interests of myo-inositol in metabolic diseases. Biochimie 2013;95:1811-1827.

56. Tominaga T, Sharma I, Fujita Y, Doi T, Wallner AK, Kanwar YS. Myo-inositol oxygenase accentuates renal tubular injury initiated by endoplasmic reticulum stress. Am J Physiol Renal Physiol 2019;316:F301-F315.

57. Sharma I, Deng F, Liao Y, Kanwar YS. Myo-inositol Oxygenase (MIOX) overexpression drives the progression of renal tubulointerstitial injury in diabetes. Diabetes 2020;69:1248-1263.

58. Martínez-Granados B, Morales JM, Rodrigo JM, et al. Metabolic profile of chronic liver disease by NMR spectroscopy of human biopsies. Int J Mol Med 2011;27:111-117.

59. Zhong F, Liu X, Zhou Q, et al. 1H NMR spectroscopy analysis of metabolites in the kidneys provides new insight into pathophysiological mechanisms: applications for treatment with Cordyceps sinensis. Nephrol Dial Transplant 2012;27:556-565.

60. Zablocki K, Miller SP, Garcia-Perez A, Burg MB. Accumulation of glycerophosphocholine (GPC) by renal cells: osmotic regulation of GPC:choline phosphodiesterase. Proc Natl Acad Sci U S A 1991;88:7820-7824.

61. Rouvière O, Yin M, Dresner MA, et al. MR elastography of the liver: Preliminary results. Radiology 2006;240:440-448.

62. Kim JK, Yuen DA, Leung G, et al. Role of magnetic resonance elastography as a noninvasive measurement tool of fibrosis in a renal allograft: A case report. Transplant Proc 2017;49:1555-1559.

63. Kirpalani A, Hashim E, Leung G, Kim JK, Krizova A, Jothy S, Deep M, Jiang nn, Glick L, Mnatzakanian G, Yuen DA. Magnetic resonance elastography to assess fibrosis in kidney allografts. Clin J Am Soc Nephrol 2017;12:1671-1679.

64. Shepherd TM, Thelwall PE, Stanisz GJ, Blackband SJ. Aldehyde fixative solutions alter the water relaxation and diffusion properties of nervous tissue. Magn Reson Med 2009;62: 26-34.

요약 (국문초록)

신 실질 질환에서 정량적 자기공명영상의 유용성: 쥐 만성 신 질환 모델을 이용한 실험연구

서울대학교 의과대학원

영상의학과

김상윤

연구 목적

아데닌을 이용한 만성 신질환 실험동물 모델을 이용하여 만성 신질환의 실질섬유화를 평가함에 있어 정량적 자기공명영상의 유용성을 검증하고 적절한 이미지 바이오 마커를 제안하고자 한다.

연구 방법

총 16 마리의 수컷 위스타 (Wistar) 쥐를 세 개의 그룹으로 나누어 – 대조군 (n=7), 만성신질환 실험군 1 (n=5), 만성신질환 실험군 2 (n=4)– 실험군의 경우, 각각 0.25% 아데닌을 3 주 또는 6 주 기간 동안 노출시켜 만성 신질환을 유발한 뒤, 9.4T 소동물 MRI 기기를 이용하여 확산강조영상 (DWI), T1ρ (T1 rho), T2*맵 (mapping), 생체 내 MR 분광분석(in vivo ^{1}H–MRS) 검사를 시행하였다. 영상 검사 후, 적출한

신장의 반정량적 조직병리학적 분석을 시행하여 만성 신질환 병리 분석 결과와 영상 분석을 통해 얻은 정량적 파라 미터 값 사이의 통계적 유의성은 검증하였다.

연구 결과

정상신을 가진 대조군과 비교하였을 때, 아데닌 노출 기간에 따라 만성 신질환의 유의한 조직병리학적 변화가 관찰되었다. 확산계수(ADC), T1ρ (T1 rho) 값은 만성신질환 실험군에서 유의한 증가를 보였다. 신장 피질(CO)과 바깥 수질(OM)에서 측정한 확산계수, T1ρ 값의 유의한 증가를 보였다. 확산계수 값은 노출 기간에 따라 증가하는 경향이 있었고, T1ρ (T1 rho) 값은 3 주 동안 노출시킨 만성신질환 실험군 1 에서 증가하다가 6 주 실험군에서는 감소하는 경향을 보였다. MR 분광분석 대사 물 가운데, 신 수질에서 얻은 myo-inositol (Ins)-glycine (Gly) 대비 콜린 (choline) 화합물 (glycerophosphorylcholine (GPC)-choline (Cho)-phosphatidylcholine (PC)의 비율이 만성신질환 실험군에서 유의하게 낮은 소견을 보였다.

결론

우리는 이 실험을 통해 정량적 MR 영상은 비 침습적인 방법으로 만성 신질환을 진단하고 평가하는 도구로서 잠재적 가능성을 확인하였다. 특히 T1ρ 은 신실질의 섬유화를 정량적으로 평가하는데 적합한 정량적 MR 시퀀스 파라 미터임을 확인하였다. 생체 내 MR 분광분석을 이용한 대사물의 변화 추적이 만성 신의 osmolality 변화를 반영하는 비침습적 방법이 될 수 있음을 확인하였다.

학번: 2011-30538